

Thermally and Optically Activated Migration of Charge Carriers in Alkali Metal Sesquioxides

Matthias Adlung,^[a] Matej Komelj,^[b] Claudia Wickleder,^{*[a]} and Martin Jansen^{*[c]}

Dedicated to Professor Peter Junk on the Occasion of his 60th Birthday

The alkali metal sesquioxides A_4O_6 ($A=K, Rb, Cs$) are mixed-valent with respect to oxygen and display several degrees of electronic and structural freedom, which give rise to diverse transport and ordering processes. We report on analyses of the respective underlying excitations by diffuse reflectance spectroscopy and thermally activated electron transport. Backed by DFT based band structure calculations we identify three possible mechanisms, inter valence charge transfer from

peroxide to superoxide, excitation across the Jahn-Teller gap of tilted superoxide anions, and polaron migration. The activation energies as found by the three different approaches are in a rather narrow range of 0.62–0.89 eV for Rb_4O_6 and 0.49–0.65 eV for Cs_4O_6 , confirming opacity in the full range of visible light. The effect of the phase transition from cubic to tetragonal as demonstrated for the caesium representative corresponds to a marginal shift to higher activation energy.

Introduction

The alkali metal sesquioxides A_4O_6 ($A=K, Rb, Cs$) constitute a small family of solids representing rare examples of mixed valency within an oxide anion substructure.^[1–3] These binary oxides display all the same electronic and structural degrees of freedom known from open shell transition metal compounds, giving rise to diverse order/disorder transitions, as there are electron localisation, charge ordering, structural relaxation, orbital ordering and spin ordering (long range magnetic order). Thus, even representing kind of a singularity, the p electron open shell alkali metal sesquioxides are of general relevance in condensed matter sciences since they offer opportunities for exploring potential correspondences with the observations made on open shell d and f electron systems.

The charge disordered state of the sesquioxides is realised in a cubic crystal system, and derives from the thorium phosphide type of structure, which can be expressed formally

as $Th_3P_4 \rightarrow (O_2)_3A_4$. Here, all oxygen atoms occupy the same Wyckoff position, thus establishing complete peroxide/superoxide disorder, i.e. charge disorder (Figure 1a).^[1,2] On cooling, a charge ordering transition takes place, which is accompanied by a diffusionless structural relaxation to a tetragonally distorted variant of the cubic structure (Figure 1b).^[4,5] Since this process is associated with a drop in electronic conductivity by more than two orders of magnitude, all phenomena taken together parallel those characterising the classical Verwey charge order transition,^[6] first reported for prototypic Fe_3O_4 .^[7] As another result of that structural reorganisation, the open shell superoxide dumbbells, $(O_2)^-$, are tilted with respect to each other, indicating orbital ordering, consistent with an intermolecular Jahn-Teller effect, lifting the degeneracy of the unequally populated π^* molecular orbitals.^[4] Recently, on cooling Rb_4O_6 further, another displacive phase transition was encountered, effecting a change in the orbital ordering scheme.^[8] Finally, only for the Rb representative, coupling of the unpaired spins at adjacent superoxide anions to spin dimers

[a] Dr. M. Adlung, Prof. Dr. C. Wickleder
Department of Chemistry and Biology
School of Science and Technology
University of Siegen, Adolf-Reichwein-Str. 2, 57068 Siegen, Germany
E-mail: wickleder@chemie.uni-siegen.de

[b] Dr. M. Komelj
Department of Nanostructured Materials
Institute Jožef Stefan
Jamova 39, 1000 Ljubljana, Slovenia

[c] Prof. Dr. Dr. M. Jansen
Max Planck Institute for Solid State Research
Heisenbergstr. 1, 70569 Stuttgart, Germany
E-mail: m.jansen@fkf.mpg.de

Supporting information for this article is available on the WWW under <https://doi.org/10.1002/cphc.202200183>

© 2022 The Authors. ChemPhysChem published by Wiley-VCH GmbH. This is an open access article under the terms of the Creative Commons Attribution Non-Commercial NoDerivs License, which permits use and distribution in any medium, provided the original work is properly cited, the use is non-commercial and no modifications or adaptations are made.

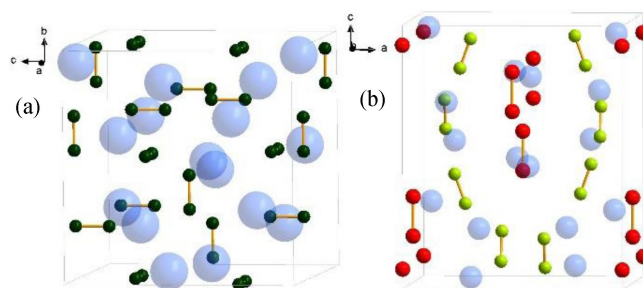


Figure 1. Illustration of the crystal structures of the cubic (left) and the tetragonal (right) polymorphs of A_4O_6 ($A=Rb, Cs$). In the cubic phase the O_2^{2-} and O_2^- units are disordered, occupying the same Wyckoff position (dark green). In the tetragonal phase the peroxide ions O_2^{2-} (red) and superoxide ions O_2^- (light green) are ordered. Cs^+ (Rb^+) ions are shown as light blue spheres.

has resulted in a fully diamagnetic ground state existing below 15 K.^[8] Still, two intriguing phenomena have remained unresolved. Depending on the strength of electron correlation, the partly populated bands might drive valence electrons itinerant, causing metallic conductivity. However, this has not yet been observed up to pressures, applied in a diamond anvil cell, of 80 GPa and 180 GPa for Rb₄O₆ and Cs₄O₆, respectively. The valence electrons stay localised at the (O₂)ⁿ⁻ dumbbells, which on their turn are disordered in the cubic phase. Further, the deep black colour of all three representatives known is hard to rationalize since they consist of colourless or pale-yellow ionic building blocks. Charge ordering in alkali metal sesquioxides is associated with a diffusionless structural phase transition from a cubic to a tetragonal crystal system implying reorientation of the diatomic oxide anions and translational movements of electrons, exclusively. Thus, mobility of the electrons, its activation and underlying mechanism, are of crucial relevance for understanding chemistry and physics of these materials. First clues into this issue are the bulk electronic conductivity measured^[6,8] and the deep black inherent colour, indicating absorption of the full range of visible light. Here we report on the results of UV/VIS/NIR spectroscopy, and a DFT based theoretical analysis.

Results

UV/VIS/NIR Reflectance Spectroscopy

For both, Rb₄O₆ (green spectrum in Figure 2) as well as Cs₄O₆ (blue spectrum in Figure 2) the reflectance spectra at room temperature consist of a pronounced absorption edge, onset at around 6200 cm⁻¹. This is corresponding to 0.77 eV for Rb₄O₆ (intersection of dashed line and solid line in Figure 2) whereas the absorption drop is slightly shifted to lower energies for Cs₄O₆ (0.68 eV, intersection of dotted line and solid line in Figure 2). These steep slopes of absorption were observed down to about 13000 cm⁻¹ and 15000 cm⁻¹, while the absorption stays on a virtually constant level between 15000 cm⁻¹ and

30000 cm⁻¹ for both compounds. Additional absorption edge starting at about 30000 cm⁻¹ was observed for all samples. The latter has been assigned undoubtedly to transitions caused by BaSO₄ (added to the specimens for the purpose of optical dilution), which was evidenced by recording the reflectance spectra of the pure compounds BaSO₄ and Cs₄O₆ (Figure S1). Thus, the low energy absorption features are caused by the alkali metal sesquioxides and can be assigned to band-band-transitions. On cooling the Cs₄O₆ specimen to 250 K, the low energy absorption edge shifts to slightly higher energy (red spectrum in Figure 2) reflecting the phase transition from the cubic to the tetragonal polymorph, and the orbital ordering associated. In addition, a relatively narrow absorption peaking at 6900 cm⁻¹ (0.86 eV) is observed, which we assign to a charge transfer between local energy levels within the band gap of O₂ⁿ⁻ units in the tetragonal phase. At warming to RT, the absorption edge shifts back to lower energy (black spectrum in Figure 2), confirming that the phase transition is reversible. Further, the additional absorption band observed at 6900 cm⁻¹ disappears. For an accurate experimental determination of the band gaps for Rb₄O₆ and cubic as well as tetragonal Cs₄O₆, Tauc-Plots were set up assuming indirect band gap transitions (Figure 3) using equation (1), which relates the absorption coefficient α and the energy of the band gap E_g ^[9]

$$(ah\nu)^{\frac{1}{n}} = B(h\nu - E_g) \quad (1)$$

h represents the Planck constant, ν the photon frequency and B a proportionality constant. The exponent n indicates the nature of the electronic transition, $n = 1/2$ for a direct allowed, $n = 2$ for an indirect allowed transition. The absorption coefficient can be expressed by the Kubelka-Munk function $F(R_\infty)$, equation (2),

$$(F(R_\infty)h\nu)^{\frac{1}{n}} = B(h\nu - E_g) \quad (2)$$

while transforming the reflectance spectra into absorption spectra,^[10] equation (3), where K and S are absorption and scattering coefficients, respectively.

$$F(R_\infty) = \frac{K}{S} = \frac{(1 - R_\infty)^2}{2R_\infty} \quad (3)$$

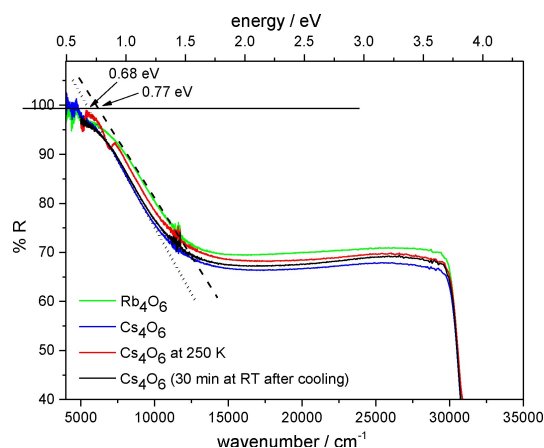


Figure 2. Reflectance spectra of Rb₄O₆ and Cs₄O₆ diluted with BaSO₄.

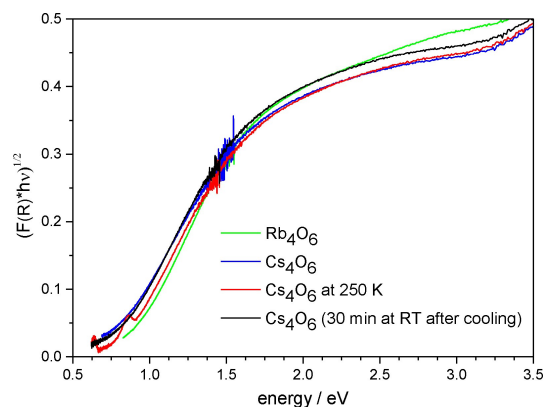


Figure 3. Tauc-Plot for indirect allowed transitions in Rb₄O₆ and Cs₄O₆.

The linear fits of the respective plots (Figure 4) resulting with $n=2$ are indicative for an indirect allowed band transition. The band gaps amount to 0.84 eV for cubic Rb_4O_6 and to 0.72 eV for cubic Cs_4O_6 , respectively, while for tetragonal Cs_4O_6 a value of 0.80 eV was obtained. After warming up and keeping at room temperature for 30 min the band gap relaxed to 0.76 eV. The absorption coefficient in the low energy range of the spectra obeys the exponential Urbach law^[11] (Figure 5) and can be calculated using the relation

$$F(R_\infty)(hv) = Ae^{hv/E_u} \quad (4)$$

where A is a constant and E_u is the Urbach-energy, which can be explained as the width of the tails of states in the band gap above and below the valence band and the conduction band, respectively. These states can be associated with structural defects (e.g. vacancies, F-centres) and/or disorder within the crystal. Here, the width of the Urbach-tail E_u was determined by the reciprocal slope of the linear fit to $E_u=0.09$ eV for Rb_4O_6 and $E_u=0.13$ eV for Cs_4O_6 , respectively. (Figure 5).

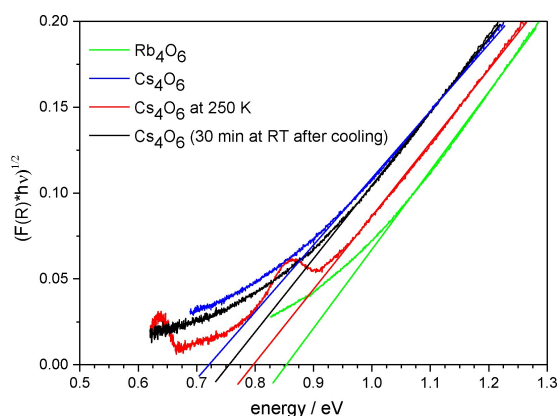


Figure 4. Determination of the band edge energies by linear fits of the Tauc-Plots for indirect allowed transitions in Rb_4O_6 and Cs_4O_6 .

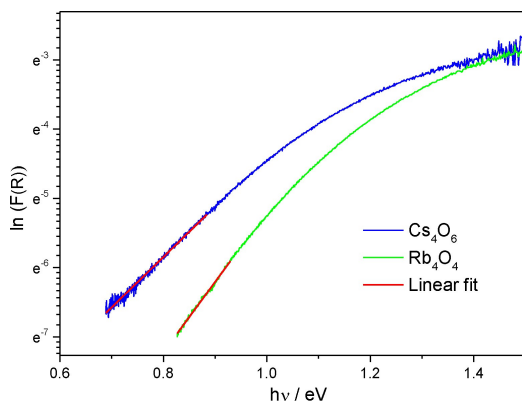


Figure 5. Determination of the Urbach-energy by a linear fit of the logarithmic plot of the Kubelka-Munk function versus hv .

Activation Energy of Bulk Electronic Conductivity

The transport properties of bulk Rb_4O_6 and Cs_4O_6 have been reported earlier in the context of studies on charge and magnetic ordering phenomena.^[6,8] Since the inter $(\text{O}_2)^{n-}$ hopping integrals are but small and the on-site electron correlations rather strong, both sesquioxides adopt an insulating ground state.^[12] The Arrhenius plots for ac conductivity, as measured by impedance spectroscopy, evidence a thermally activated behaviour (Figure 6).

In either case, the charge ordering phase transition from the cubic to tetragonal modification is associated with a drop in conductivity by two orders of magnitude. The activation energies for the cubic phases were determined as $E_A=0.62$ eV and 0.49 eV for Rb_4O_6 and Cs_4O_6 , respectively. The activation energy for the tetragonal phase is slightly increased to $E_A=0.51$ eV for Cs_4O_6 , while staying virtually unchanged for Rb_4O_6 . The pronounced hysteresis as function of temperature observed in the impedance data for both compounds reflect the martensitic nature of the cubic to tetragonal phase transition, and the concomitant variance in long range electron transport, without affecting the activation energies (band gaps) significantly. Thus, the hysteresis is not noticeable by diffuse reflectance.

Electronic Structure Calculations

For the DFT based band structure calculations the Hubbard correction (U) was applied to the p-orbitals of the oxygen atoms, which are the chemically active orbitals on the super- and peroxide anions. In earlier studies a correction between 4 and 8 eV have proven to give a reasonable description of alkali super- and peroxides.^[13,14]

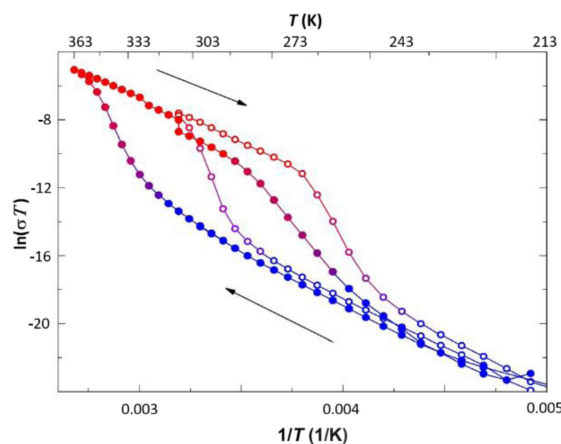


Figure 6. Bulk electronic conductivities σ (S cm^{-1}), multiplied by T , are shown as Arrhenius plots for Rb_4O_6 (closed circles) and for Cs_4O_6 (open circles).^[6,8] Arrows indicate heating and cooling modes, respectively, the colors of the symbols stand for the cubic phase (red) and for the tetragonal phase (blue). The small jumps seen in the cooling mode for Rb_4O_6 are artefacts due to changes of electrical contact at varying the temperature.

However, the choice of the U value is not unique, and it depends on the investigated system (in this case, on the type of the alkali ion) as well as on the implementation of the U correction. A comparison with the measured band structure gaps yields $U=3.7$ eV and $U=4.1$ eV as the optimum values in the case of Rb_4O_6 and Cs_4O_6 , respectively; for the applied U -correction scheme see ref. [15]. Figures 7 and 8 represent the calculated density-of-states plots for Rb_4O_6 and Cs_4O_6 , respectively.

It is evident that the O-p states are the most relevant around the Fermi level, whereas the s contribution of the metallic ions is almost negligible. In both, the Rb and Cs systems, the lowest unoccupied states almost exclusively belong to the O_2^- dumb-bells. However, there is a noticeable difference in the population of the Fermi level between the Rb_4O_6 and Cs_4O_6 systems.

Whereas the former is mainly populated by the O_2^- electrons, the O_2^{2-} electrons dominate in the latter hinting that the excitations across the Jahn-Teller gap are more pronounced in Rb_4O_6 , similar to the scenario proposed for the alkali-metal superoxide KO_2 .^[13] However, the occupied peroxide band is significantly broader for Rb_4O_6 than for Cs_4O_6 and extends

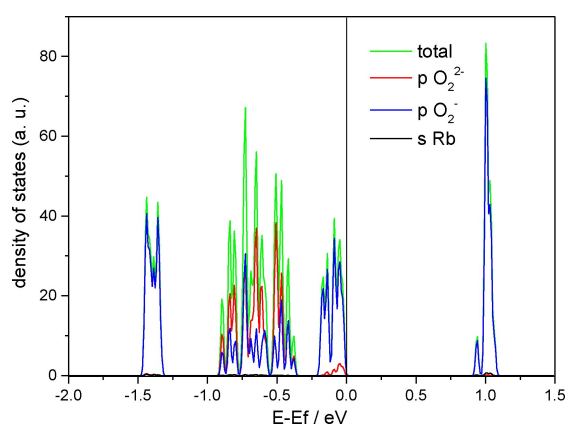


Figure 7. The calculated total, p-resolved O, and s-resolved Rb densities of states for Rb_4O_6 .

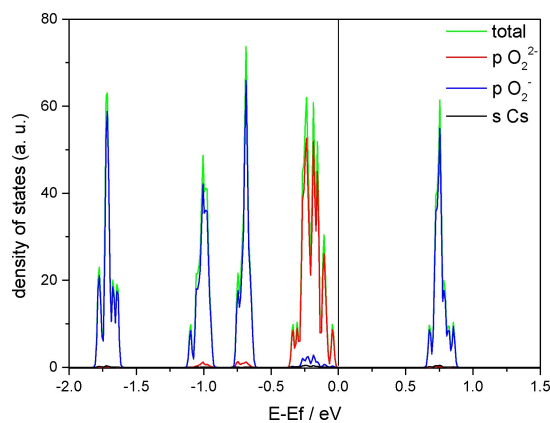


Figure 8. The calculated total, p-resolved O, and s-resolved Cs density of states for Cs_4O_6 .

below the respective occupied p_x/p_y bands of O_2^- . Splitting between the occupied peroxide and unoccupied superoxide states in Cs_4O_6 is smaller, therefore the corresponding electron transfer is lower in energy. According to the calculated density of states and band structure, such transfer is relevant for Rb_4O_6 , too, however, it is superimposed by an excitation across the Jahn-Teller gap for the superoxide anions. A more detailed insight into the electronic levels is given in terms of the band structures, Figures 9 and 10. The topologies of the lowest unoccupied bands in both systems are very similar, except that they are slightly narrower in the case of Rb_4O_6 .

The difference is more pronounced for the bands below the Fermi level. Cs_4O_6 clearly exhibits a direct gap, whereas a slightly indirect gap in Rb_4O_6 might result in a weaker absorption. The intriguing difference between the band structures of the two systems might be to some extent ascribed to the difference in the lattice parameters and consequently to the influence of the crystal field acting on the oxygen dumb-bells. Due to the smaller lattice parameter, the effect of the crystal field is more pronounced in Rb_4O_6 than in Cs_4O_6 , making the O_2^{2-} anions in the former more stable, which is reflected in lower energies of the corresponding occupied states, as it is evident from the calculated density of states. For the same reason the empirically determined Hubbard U value is lower for

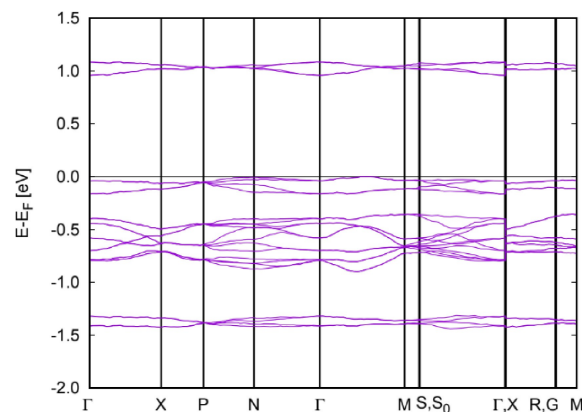


Figure 9. The calculated Rb_4O_6 band structure.

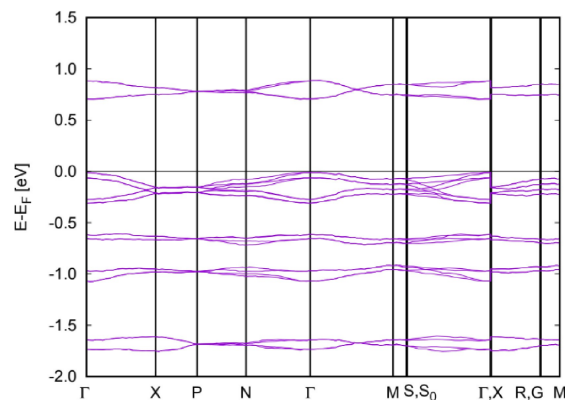


Figure 10. The calculated Cs_4O_6 band structure.

the system with a stronger crystal field, in accordance with the experimentally obtained band gap. To prove this hypothesis, we performed a calculation for the Cs_4O_6 system with the Rb_4O_6 lattice parameters. The result is indeed a band structure which reproduces some of the Rb_4O_6 key features including the band gap and the position of the highest occupied O_2^{2-} states.

Discussion

The alkali metal sesquioxides can be regarded as basically ionic compounds, consisting of alkali metal cations and diatomic anionic species, i.e., all valence electrons are located in the 2p derived π and π^* type molecular orbitals of oxygen. Thus, the mixed-valency displayed, the unique physical properties and ordering phenomena like the Verwey type charge ordering on the anionic sublattice^[6] and spin dimers constituting the magnetically ordered ground state^[8] are driven by electronic processes between and within the diatomic oxygen species. Obviously, for any kind of microscopic understanding of the phenomena mentioned, knowledge of electron mobilities and activation thresholds constitute a crucial condition. On the timescale of vibrational spectroscopy, the electrons appear localized,^[16] corresponding to minimal lifetimes in the range of 100 fs to 1 ns, even if the charges of the diatomic oxygen species are disordered, e.g. in the cubic polymorphs. As recorded by impedance spectroscopy, the charge transfer within the cubic modifications takes place at a mobility of $u(298\text{ K}) \approx 10^{-9} \text{ cm}^2/(\text{Vs})$ ^[6,8] determining the border line for the thermally activated dynamics of electron migration.

Computational analyses of the electronic structures of alkali metal sesquioxides have proven to be challenging, mainly due to uncertainties and lacking experience in proper treatment of electron correlations. In an early study based on density functional calculations within the local spin density approximation, half-metallic ferromagnetism and a magnetic ordering temperature of 302 K was predicted,^[17] which later has been shown to be at odds with experiment.^[18] Subsequent calculations correctly reproduced the semiconducting nature, however failed to predict the true magnetic exchange pattern.^[12] Based on knowledge of the charge ordered crystal structures^[4] and an appropriate choice of the Hubbard U , optical and thermal excitations in terms of DFT band structure calculations, UV/VIS/NIR and impedance spectroscopy have produced quite consistent results, in the study presented here.

The band structures of the tetragonal phases feature rather flat bands throughout and are underlining the pronounced localization of the valence electrons in the π and π^* type MOs as well as the ionic character of the compounds. Accordingly, the relevant bands around the Fermi level are prevalingly of oxygen nature, while the alkali metal s electron related states are virtually irrelevant. Three optically and thermally activated processes can be assigned, inter-valence charge transfer (IVCT) $(\text{O}_2)^{2-} \rightarrow (\text{O}_2)^-$, excitation across the Jahn-Teller gap opened by lifting the degeneracy of the π^* type MO of $(\text{O}_2)^-$ in the tetragonal low temperature polymorph, and polaron migration. As to be expected, the topologies of the band structures of the

rubidium and cesium representatives are similar. Yet the oxygen p type bands are shifted against each other, which is basically a consequence of the stabilisation of the peroxide anion in Rb_4O_6 due to the stronger crystal field in comparison to the Cs analogue. Among the possible transitions, the IVCT process contributes to long-range electron transport, but the contribution by a hole (electron) polaron migration should also be considered, as suggested by the fact that thermal activation energies found from conductivity measurements are slightly different from those obtained from UV/VIS/NIR, see Table 1. Therefore, we cannot rule out that the microscopic mechanisms for thermal and optical excitations are different. Especially as the Urbach tails seen by reflection spectroscopy indicate presence of inter band gap defect states above and below the valence band and conduction band. A thermally activated charge transport could proceed preferentially via defect states, while an optical activation would tend to a transfer directly into the conduction band at higher energies.

Basically, all findings are in accordance with the classical model for semiconductors, reflecting a gapped band structure, where thermal as well as optical excitations are enabling electron transport. However, this picture is not suited to provide an explicit understanding of the microscopic mechanism underlying the long-range electron transport or, to put it more correctly, polaron migration. At a first glance, the long intermolecular distances of about 3.30 Å would exclude to assume some direct intermolecular $(\text{O}_2)^{n-}$ interactions, since this distance coincides with the so-called van der Waals peak^[19] were a maximum in the number of non-interacting O–O separations is observed in experimental data. However, the magnetic dimer coupling to happen across an intermolecular O–O separation as wide as 3.27 Å^[8] encourages to assume existence of a small, however, finite hopping integral. Accepting this assumption would admit assigning the system as mixed valence of type II according to the classification by Robin and Day.^[20]

Conclusions

In summary, for Cs_4O_6 the relevant transitions dominating optical absorption and activation of polaron migration correspond to a plain IVCT from $(\text{O}_2)^{2-}$ to $(\text{O}_2)^-$. For Rb_4O_6 , however, the IVCT appears to be superimposed by a vertical excitation across the Jahn-Teller gap, $\pi^*(x) \rightarrow \pi^*(y)$.

Table 1. Activation energy of the electronic conductivity (E_{ae}), energy of the optical band gap (E_g) and the theoretical band gap (E_{gt}) in eV for the C-Phase (C) and T-phase (T).

	E_{ae}	E_g	E_{gt}
Rb_4O_6	0.62 (C)	0.84 (C)/	0.89 (T)
Cs_4O_6	0.49 (C)/0.51 (T)	0.72 (C)/0.8 (T)	0.65 (T)

Experimental Section

Source of Materials

Rb₄O₆ and Cs₄O₆ were synthesized as micro-crystalline powders starting from the respective superoxides by controlled thermal degradation. A detailed prescription is published elsewhere.^[21] Phase purity and identity of the samples investigated were confirmed by le Bail fits to the X-ray powder diffractograms, see Figure 11.

Reflectance spectra were measured with an UV/VIS/NIR photometer Cary 5000 from Varian (Agilent Technology) equipped with an integration sphere for diffuse reflectance measurements. The deep black pristine sesquioxides were diluted with BaSO₄ in a ratio of 1:20 to 1:30 to avoid excessive absorption. Furthermore, samples of Cs₄O₆ were cooled for one day at 250 K to investigate the tetragonal phase additionally to the cubic one. All samples were prepared in an Ar-glove box and inserted in a home-built, airtight cell for measurements.

Impedance Spectroscopy

All conductivity data included in this report are taken from earlier work on Rb₄O₆^[8] and Cs₄O₆^[6], all experimental details are given in the respective supplementary informations.

Computational Details

The band structure calculations were performed in the framework of the density-functional theory (DFT) by applying the Quantum Espresso code^[22] for the experimentally-determined^[6,8] structures of the tetragonal phases (Tables S1 and S2). The exchange-correlation effects were calculated in the generalized-gradient approximation^[23] with explicitly added Coulomb-repulsion *U* term for the oxygen *p* states. The electron-ion interactions were described with the norm-conserving pseudopotentials. The plane-waves and charge-density cut-off parameters were set to 639 eV and 2543 eV, respectively, and a 3×3×3 k-points meshes were

used for the Brillouin-zone integration. The self-consistent criterion was the total-energy difference between the two subsequent iterations being less than 10⁻⁶ Ry. The anti-ferromagnetic ordering of the O₂⁻ dumbbells was considered. The *U* parameters were determined empirically in order to achieve an agreement with the experimental results, which yielded *U* = 3.7 eV for the Rb, and *U* = 4.8 eV for the Cs system. Since for the considered magnetic ordering the difference in densities of states and the band structures for the two spin channels are very subtle, we do not make the distinction in the corresponding graphs.

Acknowledgements

We thank Patrick Merz for synthesizing the sesquioxides samples, and Gohil S. Thakur for performing the PXRD le Bail fits. Open Access funding enabled and organized by Projekt DEAL.

Conflict of Interest

The authors declare no conflict of interest.

Data Availability Statement

The data that support the findings of this study are available from the corresponding author upon reasonable request.

Keywords: inter valence charge transfer · mixed valency oxide · optical excitation · polaron migration · UV/Vis spectroscopy

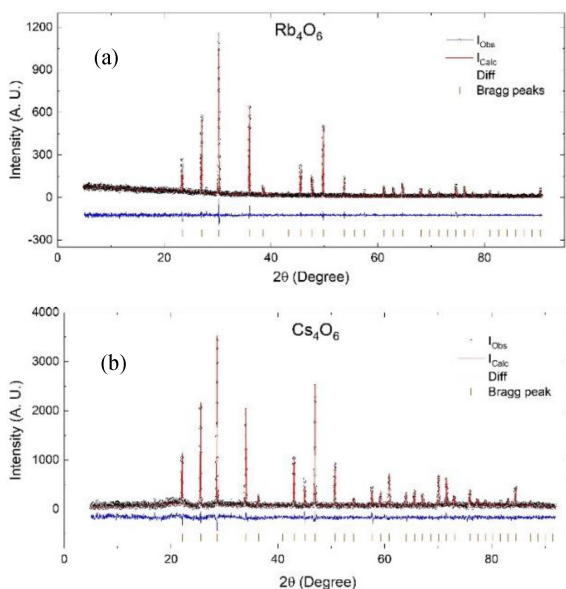


Figure 11. Le Bail fits to the room temperature X-ray powder diffractograms of Rb₄O₆ (a) and Cs₄O₆ (b).

- [1] A. Helms, W. Klemm, *Z. Anorg. Allg. Chem.* **1939**, *242*, 201–214.
- [2] M. Jansen, N. Korber, *Z. Anorg. Allg. Chem.* **1991**, *598*, 163–173.
- [3] C. Freysoldt, P. Merz, M. Schmidt, S. Mohitkar, C. Felser, J. Neugebauer, M. Jansen, *Angew. Chem. Int. Ed.* **2019**, *58*, 143–153.
- [4] A. Sans, J. Nuss, G. H. Fecher, C. Mühle, C. Felser, M. Jansen, *Z. Anorg. Allg. Chem.* **2014**, *640*, 1239–1246.
- [5] R. H. Colman, H. E. Okur, W. Kockelmann, C. M. Brown, A. Sans, C. Felser, M. Jansen, K. Prassides, *Inorg. Chem.* **2019**, *58*, 14532–14541.
- [6] P. Adler, P. Jeglič, M. Reehuis, M. Geiß, P. Merz, T. Knaflič, M. Komelj, A. Hoser, A. Sans, J. Janek, et al., *Sci. Adv.* **2018**, *4*, eaap7581.
- [7] E. J. W. Verwey, *Nature* **1939**, *144*, 327–328.
- [8] T. Knaflič, P. Jeglič, M. Komelj, A. Zorko, P. K. Biswas, A. N. Ponomaryov, S. A. Zvyagin, M. Reehuis, A. Hoser, M. Geiß, et al., *Phys. Rev. B* **2020**, *101*, 591.
- [9] B. D. Viezbigke, S. Patel, B. E. Davis, D. P. Birnie, *Phys. Status Solidi B* **2015**, *252*, 1700–1710.
- [10] P. Makula, M. Pacia, W. Macyk, *J. Phys. Chem. Lett.* **2018**, *9*, 6814–6817.
- [11] a) F. Urbach, *Phys. Rev.* **1953**, *92*, 1324; b) R. Bhatt, I. Bhaumik, S. Ganesamoorthy, A. K. Karnal, M. K. Swami, H. S. Patel, P. K. Gupta, *Phys. Status Solidi A* **2012**, *209*, 176–180; c) J. I. Pankove, *Phys. Rev.* **1965**, *140*, A2059–A2065.
- [12] J. Winterlik, G. H. Fecher, C. A. Jenkins, C. Felser, C. Mühle, K. Doll, M. Jansen, L. M. Sandratskii, J. Kübler, *Phys. Rev. Lett.* **2009**, *102*, 16401.
- [13] N. R. Mathiesen, S. Yang, J. M. García-Lastra, T. Vegge, D. J. Siegel, *Chem. Mater.* **2019**, *31*, 9156–9167.
- [14] a) M. Kim, B. I. Min, *Phys. Rev. B* **2014**, *89*; b) A. K. Nandy, P. Mahadevan, P. Sen, D. D. Sarma, *Phys. Rev. Lett.* **2010**, *105*, 56403; c) R. Christensen, J. S. Hummelshøj, H. A. Hansen, T. Vegge, *J. Phys. Chem. C* **2015**, *119*, 17596–17601.
- [15] M. Cococcioni, S. de Gironcoli, *Phys. Rev. B* **2005**, *71*, 16.
- [16] a) M. Jansen, R. Hagenmayer, N. Korber, *C. R. Acad. Sci. Ser. IIC* **1999**, *2*, 591–594; b) J. Winterlik, G. H. Fecher, C. A. Jenkins, S. Medvedev, C.

- Felser, J. Kübler, C. Mühle, K. Doll, M. Jansen, T. Palasyuk, et al., *Phys. Rev. B* **2009**, *79*, 591.
- [17] J. J. Attema, G. A. de Wijs, G. R. Blake, R. A. de Groot, *J. Am. Chem. Soc.* **2005**, *127*, 16325–16328.
- [18] J. Winterlik, G. H. Fecher, C. Felser, C. Mühle, M. Jansen, *J. Am. Chem. Soc.* **2007**, *129*, 6990–6991.
- [19] S. Alvarez, *Dalton Trans.* **2013**, *42*, 8617–8636.
- [20] a) M. B. Robin, P. Day, *Adv. Inorg. Chem.* **1968**; *10*, 247–422; b) M. Parthey, M. Kaupp, *Chem. Soc. Rev.* **2014**, *43*, 5067–5088.
- [21] P. Merz, M. Schmidt, C. Felser, M. Jansen, *Z. Anorg. Allg. Chem.* **2017**, *643*, 544–547.
- [22] P. Giannozzi, S. Baroni, N. Bonini, M. Calandra, R. Car, C. Cavazzoni, D. Ceresoli, G. L. Chiarotti, M. Cococcioni, I. Dabo, *J. Phys. Condens. Matter* **2009**, *21*, 395502.
- [23] Perdew, Burke, Ernzerhof, *Phys. Rev. Lett.* **1996**, *77*, 3865–3868.

Manuscript received: March 20, 2022
Revised manuscript received: May 5, 2022
Accepted manuscript online: May 5, 2022
Version of record online: May 26, 2022